


Article

Immobilization of Perylenetetracarboxylic Dianhydride on Al₂O₃ for Efficiently Photocatalytic Sulfide Oxidation

Jiahao Liang^{1,2}, Jie Wang^{1,2,*}, Hao Hou^{1,2}, Qingzhu Xu^{1,2}, Wei Liu^{1,2}, Chenliang Su^{1,2} and Hongli Sun^{1,2,*}

- ¹ International Collaborative Laboratory of 2D Materials for Optoelectronic Science & Technology, Engineering Technology Research Center for 2D Materials Information Functional Devices and Systems of Guangdong Province, Institute of Microscale Optoelectronics, Shenzhen University, Shenzhen 518060, China; 18844536117@163.com (J.L.); houhao@szu.edu.cn (H.H.); mz120210747@yzu.edu.cn (Q.X.); lw0584@szu.edu.cn (W.L.); chmsuc@szu.edu.cn (C.S.)
- ² State Key Laboratory of Radio Frequency Heterogeneous Integration, Shenzhen University, Shenzhen 518060, China
- * Correspondence: wangjie415@szu.edu.cn (J.W.); hlsun@szu.edu.cn (H.S.)

Abstract: Perylenetetracarboxylic dianhydride (PTCDA) derivatives have received significant attention as molecule photocatalysts. However, the poor recyclability of molecule-type photocatalysts hinders their widespread applications. Herein, immobilization of PTCDA on Al₂O₃ was achieved by simply physical mixing, which not only dramatically improved their recyclability, but also surprisingly improved the reactivity. A mechanism study suggested that the photo-excited state (PTCDA*) of PTCDA could promote the oxidation of thioanisole to generate PTCDA^{•−}, which sequentially reduces oxygen to furnish superoxide radicals to achieve the catalytic cycle. Herein, the immobilization support Al₂O₃ was able to facilitate the strong adsorption of thioanisole, thereby boosting the photocatalytic activity. This work provides a new insight that the immobilization of organic molecular photocatalysts on those supports with proper adsorption sites could furnish highly efficient, stable, and recyclable molecular-based heterogeneous photocatalysts.

Keywords: heterogeneous organic photocatalysts; photoredox; O₂ reduction; strong adsorption of thioanisole; thioanisole oxidation



Citation: Liang, J.; Wang, J.; Hou, H.; Xu, Q.; Liu, W.; Su, C.; Sun, H.

Immobilization of Perylenetetracarboxylic Dianhydride on Al₂O₃ for Efficiently Photocatalytic Sulfide Oxidation. *Molecules* **2024**, *29*, 1934. <https://doi.org/10.3390/molecules29091934>

Received: 2 April 2024
Revised: 19 April 2024
Accepted: 22 April 2024
Published: 24 April 2024



Copyright: © 2024 by the authors. Licensee MDPI, Basel, Switzerland. This article is an open access article distributed under the terms and conditions of the Creative Commons Attribution (CC BY) license (<https://creativecommons.org/licenses/by/4.0/>).

1. Introduction

Photoredox catalytic organic reactions have attracted increasing attention [1]. Photoredox catalysts, mainly including metal complexes, dye molecules, and polymers, have been widely applied in many classic redox reactions (dehydrogenation, carbonyl reduction, and alcohol oxidation etc.) [2]. 3,4,9,10-Perylenetetracarboxylic dianhydride (PTCDA), as one of the molecule-type photoredox catalysts, features a broad light absorption range and suitable redox property, which can achieve dehalogenation reactions, aerobic oxidation reactions, etc. [1,3]. A typical example is that PTCDA molecules can simultaneously achieve the oxidation of alcohols and the reduction of protons to release H₂ [3]. In addition, the imines derived from PTCDA can also serve as photocatalysts for dye degradation, wastewater treatment, etc. [4–8]. However, since PTCDA is a molecule photocatalyst, it is inevitable that issues such as photo-stability and difficulty will be encountered in catalyst separation and recovery. Therefore, improving its stability and recyclability by heterogenization, and still retaining and even improving its redox capabilities, is highly attractive. There are three main categories of heterogenization methods: the first one is to construct polymer/supramolecules semiconductors via pyrolysis etc. using PTCDA and its derivatives as precursors [9,10]; the second is to combine PTCDA-converted polymers/supramolecules with oxides [11–14]; and the third is to act as the functional monomers to modify the other polymers [15,16]. In the second strategy, the interaction between the PTCDA-based materials and the oxide is potentially highly important, but rarely explored. Thus, herein,

we wish to immobilize PTCDA on oxides (e.g., Al_2O_3) and probe the catalytic effects of their interaction. Specifically, a simple grinding method was used to physically mix PTCDA with metal oxides, where Al_2O_3 was screened out as a proper support for PTCDA in Figure S1. As revealed by the XPS analysis and theoretical studies, this simple grinding procedure could induce strong interaction between the anhydride groups of PTCDA and Al_2O_3 . FTIR analysis reflected that Al_2O_3 with Lewis acidity could provide sufficient molecular adsorption sites for reagents. Benefiting from the synergistic effects between PTCDA and Al_2O_3 , the photocatalytic activity of PTCDA/ Al_2O_3 was significantly higher than that of PTCDA. A mechanism study suggested that this immobilization strategy helps to enhance the absorption of reagents such as thioanisole, accelerate its conversion to the corresponding radicals, and thus promote the subsequent oxidation by the superoxide radicals from oxygen reduction.

2. Results and Discussion

2.1. Synthesis, Activity Evaluation, and Interaction Study of PTCDA/ Al_2O_3 Mixture

Al_2O_3 , as an insulator with surface hydroxyl and Lewis acid sites [17,18], was screened out as a superior support for PTCDA (Figure S1), as it can provide synergistic sites for both O_2 and substrates. The preparation of PTCDA/ Al_2O_3 (physical mixture) is shown in Figure 1a. Through the TEM images of Al_2O_3 and PTCDA in Figure 1b, Al_2O_3 exhibited a layer morphology, while PTCDA had a rod-shaped morphology. And a crystal plane spacing of 0.162 nm was displayed, belonging to the (422) plane of Al_2O_3 . After the physical mixture of Al_2O_3 and PTCDA was grounded, the rod-shaped PTCDA disappeared and was replaced by a morphology similar to Al_2O_3 . It could be observed from HRTEM images (Figure 1b, iv) that there were certain amorphous substances on the surface of Al_2O_3 , which could be classified as PTCDA molecules. EDS mapping also demonstrated the uniform distribution of PTCDA on the surface of Al_2O_3 . The XRD patterns in Figure 1c confirmed that the diffraction peaks of PTCDA molecules gradually increased as the amount of PTCDA molecules increased, demonstrating the successful incorporation of PTCDA molecules into Al_2O_3 . UV-Vis spectra reflected the light absorption properties of PTCDA and Al_2O_3 (Figure S2). Compared with Al_2O_3 , PTCDA has significant absorption within the visible light absorption range, implying that this heterogenization strategy has the potential to improve the photocatalytic activity of PTCDA/ Al_2O_3 (physical mixture). According to the reported literature [3], the reduction potential (-0.27 V vs. NHE, pH = 0) of PTCDA is more negative than that (-0.13 V vs. NHE, pH = 0) of $\text{O}_2/\bullet\text{O}_2^-$, suggesting the possibility and feasibility of activating oxygen after mixing PTCDA and Al_2O_3 . Subsequently, the photocatalytic activities toward selective oxidation of sulfide over the series of catalysts were evaluated (Figure 1d). Compared to independent Al_2O_3 or PTCDA, the heterogenized PTCDA showed a significant improvement in photocatalytic activity, where 5%PTCDA/ Al_2O_3 gave the best performance.

To understand the reasons behind the unexpectedly boosted performance of the heterogenized PTCDA, the interaction between the PTCDA and Al_2O_3 was further investigated by FTIR (Figure 1d). Compared with pure PTCDA, the bands of C=O and C–O of heterogenized PTCDA showed significant red shifts, while there were no significant shifts in C–H or C=C, confirming that the interaction was likely to occur between the anhydride group of PTCDA and Al_2O_3 . In great contrast to the minor shift of hydroxyl groups in calcinated Al_2O_3 , the significant blue shift of hydroxyl groups induced by the calcination of the PTCDA/ Al_2O_3 (physical mixture) and the apparent red shift in the characteristic infrared peaks of C=O and C–O, further confirmed that the anhydride group of PTCDA mainly interacted with the hydroxyl groups on the surface of Al_2O_3 (Figure S3). The interaction between the two was also studied by XPS (Figure 2a–c). Differently from the basically unchanged binding energy of C 1s in C–C or C=C, the binding energies of O 1s and C 1s in C–O–C and C=O decreased, and the binding energy of Al 2p increased, confirming that the mutual interaction would increase the electron density of PTCDA molecules and decrease the electron density on the surface of Al_2O_3 due to the electron-pulling effect

of the anhydride group after the interaction. The calculated differential charge density (yellow) represents an increase in charge density, while cyan represents a decrease in charge density in Figure 2d. It was also demonstrated that the adsorption on the Al_2O_3 surface would increase the electron density of PTCDA molecules, as is consistent with the results of XPS.

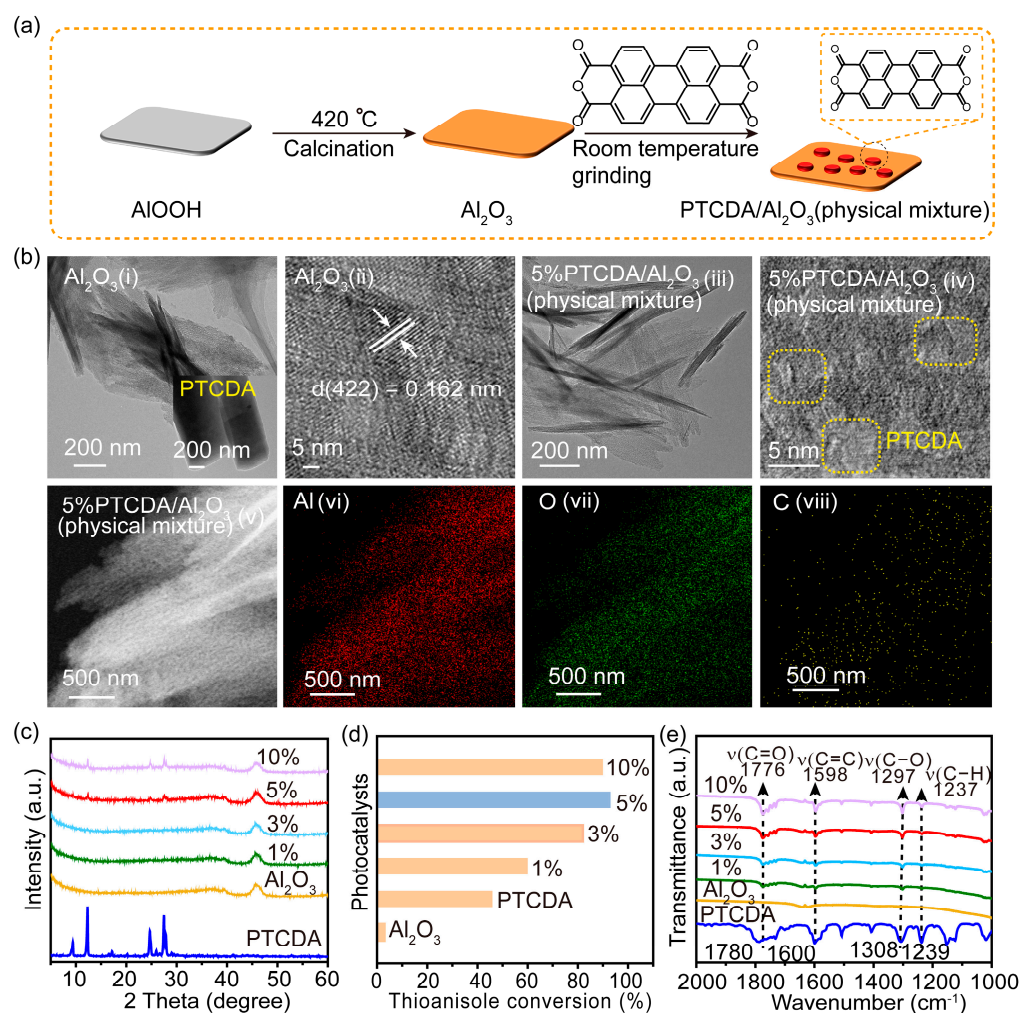


Figure 1. (a) The preparation scheme of PTCDA/Al₂O₃(physical mixture). (b) TEM (i,iii), and HRTEM (ii,iv) images of Al₂O₃ and PTCDA/Al₂O₃ (physical mixture); the insert is the image of original PTCDA. EDS mapping images (v–viii) of PTCDA/Al₂O₃ (physical mixture). (c) XRD patterns, (d) The photocatalytic activities and (e) FTIR spectra of PTCDA, Al₂O₃, and PTCDA/Al₂O₃ (physical mixture) with different mass ratios of PTCDA. Reaction conditions: photocatalyst, 10 mg; methanol, 2 mL; 0.1 mmol, thioanisole; white LED (≥ 420 nm), 500 mW cm⁻²; O₂, 1 atm; time, 5 h.

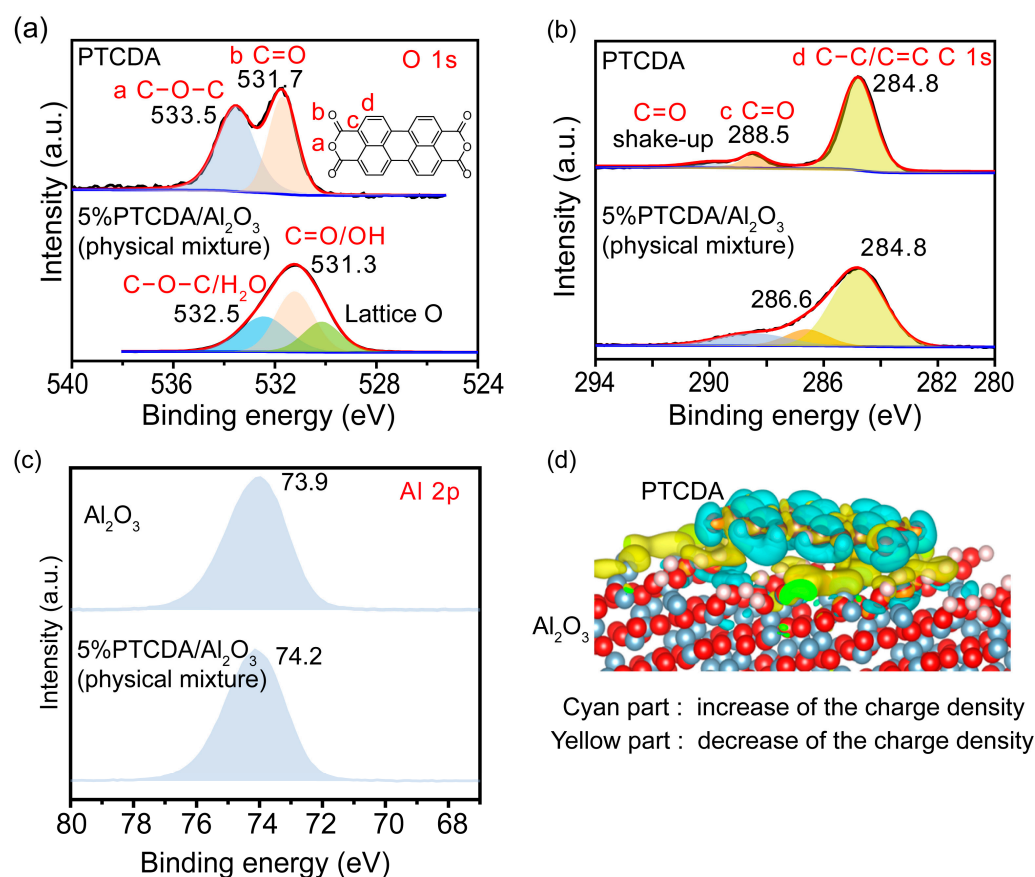


Figure 2. High-resolution XPS spectra of (a) O 1s, (b) C 1s, and (c) Al 2p for 5%PTCDA/Al₂O₃ (physical mixture) and PTCDA or Al₂O₃. (d) The calculated differential charges of PTCDA on Al₂O₃ surface.

2.2. Exploration of the Mechanism

Scavenger studies were conducted to determine the effects of various reactive species (Figure 3a). The phenomenon of almost no activity under an argon atmosphere proved the importance of oxygen. Furthermore, the quenching of ¹O₂ and •OH did not induce an obvious reduction in activity, indicating that these two oxygen reactive species were not involved in the oxidation reaction. Instead, the addition of •O₂[−] sacrificial agents significantly reduced the reaction activity, confirming that •O₂[−] was the main active species in the reaction system. Even though the •O₂[−] radicals were important in the reaction system, the intensity of •O₂[−] signals of PTCDA and heterogenized PTCDA under visible light irradiation (Figure 3b) were similar, indicating that the enhanced performances probably did not originate only from oxygen-reduction parts. We thus started to probe the influence of substrate oxidation using methanol as a probing reagent, and the Nash detection method was used to detect the presence of formaldehyde. It was found that the formaldehyde generated by the PTCDA/Al₂O₃ (physical mixture) system was 6 times higher than that of the PTCDA system, confirming that the oxidation parts were also accelerated. To further understand the remarkable enhancement, the methanol adsorption experiments were studied by FTIR (Figure S4). Classical and weak absorption peak of −CH_x of methanol was observed over Al₂O₃ and 5%PTCDA/Al₂O₃ (physical mixture), but not over PTCDA, indicating the preferential adsorption of methanol on the surface of Al₂O₃ compared to PTCDA. Similarly, the enhanced adsorption of thioanisole on 5%PTCDA/Al₂O₃ (physical mixture) was also observed (Figure 3d). Thus, it can be deduced that in the heterogenized mixture, Al₂O₃ would favor the adsorption of substrate, and PTCDA could activate O₂ to furnish •O₂[−] radicals, then work synergistically to boost the oxidation activity of sulfide. Therefore, a reasonable mechanism was proposed (Figure 3e). Under visible light irradi-

ation, PTCDA could be excited to the excited state, PTCDA*, which had the potential to oxidize the surface-adsorbed sulfide to corresponding intermediate radical 1, and itself was converted to PTCDA^{•-}. Then, O₂ could obtain electrons from PTCDA^{•-} to produce [•]O₂⁻ and further oxidize intermediate 1 to intermediate 2, then follow proton abstraction to produce sulfoxide. Table 1 shows the reaction scope. The substrate-bearing electron donating or weak electron-withdrawing groups all gave high conversion rates and yields for production of the corresponding sulfoxides. And 1 g of thioanisole was used as a substrate to conduct the large-scale photocatalytic reaction under visible light irradiation. The conversion (92%) of thioanisole and yield (62%) of benzyl sulfoxide are given in Table S2, indicating that substrate could be scaled up to the gram level. There was no significant change in photocatalytic activity after multiple cycles (Figure S5a), and FIIR spectra (Figure S5b) confirmed its stability. Overall, the heterogenized PTCDA photocatalysts exhibited good universality and excellent recyclability.

Table 1. Universality study over 5%PTCDA/Al₂O₃ (physical mixture).

Entry	Substrates	Products	Time (h)	Conv. (%)	Sulfoxide Yield(%)
1			6	93	68
2			6	94	69
3			6	99	94
4			6	91	72
5			6	94	79
6			6	96	79
7			8	91	47
8			8	96	64

Reaction conditions: Photocatalyst, 10 mg; methanol, 2 mL; substrate, 0.1 mmol; white LED (≥ 420 nm), 500 mW cm⁻²; O₂, 1 atm. The conversion and yield of benzyl sulfoxide was determined by GC-MS with anisole as internal standard. The conversion and yield of other products was determined by ¹H NMR spectra with 1,3,5-trimethylbenzene as internal standard.

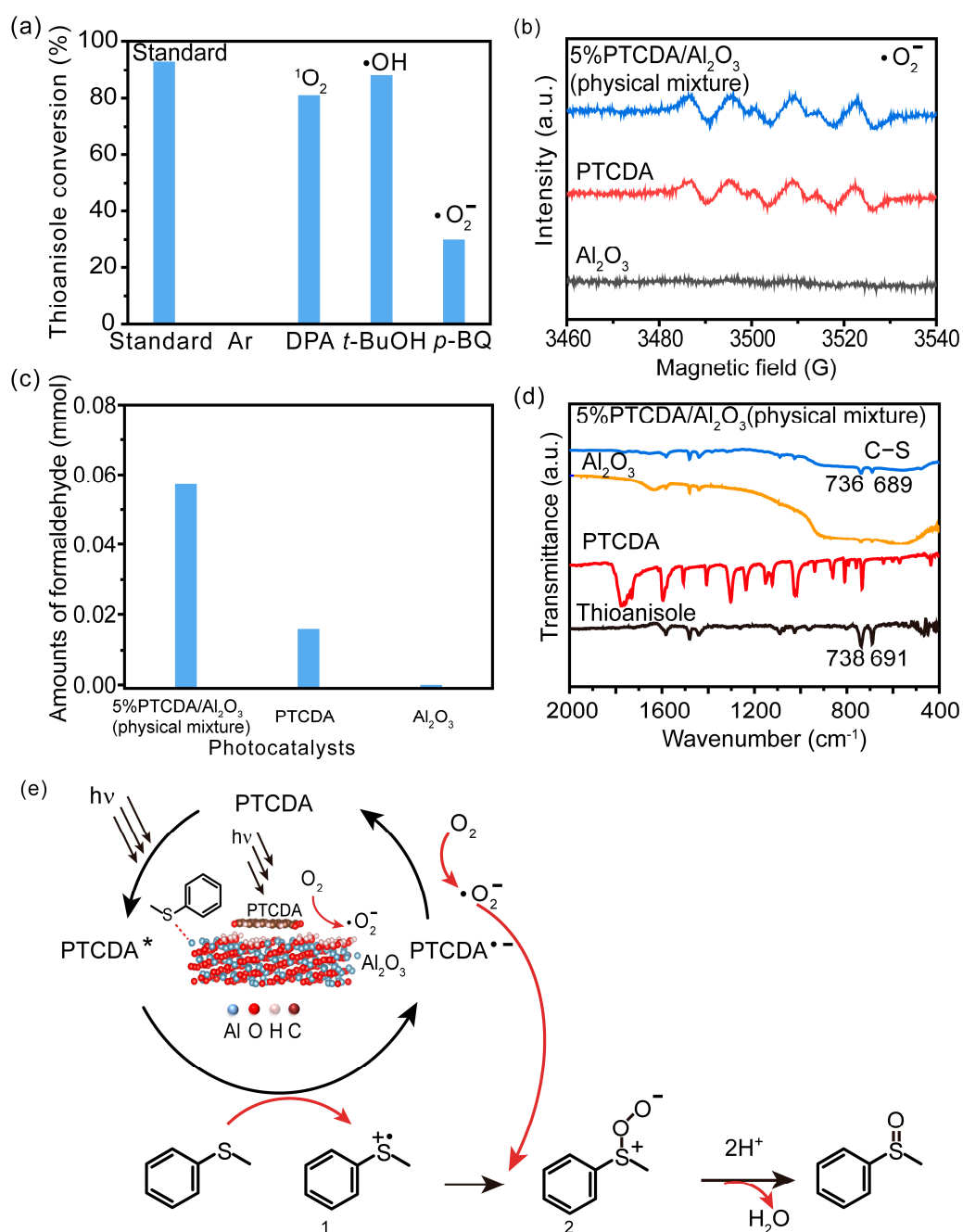


Figure 3. (a) The influence of different sacrificial agents on photocatalytic performances. *t*-butyl alcohol (*t*-BuOH), nitrotetrazolium blue chloride (NBT), and 9,10-diphenylanthrene (DPA) were used as the sacrificial agents to probe the roles of hydroxyl radical (•OH), superoxide radical (•O₂⁻), and singlet oxygen (¹O₂), respectively [19]. (b) EPR signals of the photocatalytically generated DMPO-•O₂⁻ over Al₂O₃, PTCDA, and 5%PTCDA/Al₂O₃(physical mixture). (c) The effects of different catalysts on formaldehyde production. Reaction conditions: photocatalyst, 10 mg; methanol, 2 mL; white LED (≥420 nm), 500 mW cm⁻²; O₂, 1 atm. (d) FTIR spectra of Al₂O₃, PTCDA, and 5%PTCDA/Al₂O₃ (physical mixture) after adsorbing thioanisole. (e) The proposed mechanism of thioanisole oxidation over 5%PTCDA/Al₂O₃ (physical mixture).

3. Materials and Methods

3.1. Reagents and Solvents

Aluminum nitrate nonahydrate ($\text{Al}(\text{NO}_3)_3 \cdot 9\text{H}_2\text{O}$), urea, 3,4,9,10-perylene tetracarboxylic dianhydride (PTCDA, 98%), anisole, methanol, and thioanisole were all purchased from Energy Chemical and used without further purification.

3.2. Preparation of 2D Al_2O_3 Nanosheets as Precursor

Two-dimensional Al_2O_3 nanosheets were prepared using a hydrothermal method with $\text{Al}(\text{NO}_3)_3 \cdot 9\text{H}_2\text{O}$ as raw material [18,20]. A total of 4.5 g of $\text{Al}(\text{NO}_3)_3 \cdot 9\text{H}_2\text{O}$ and 5.1 g of urea were added to a 250 mL round bottom flask, and then 250 mL of ultrapure water was added and maintained at 150 °C for 24 h to obtain a white precipitate. After cooling, the obtained white precipitate was washed with ultrapure water to pH = 7.0 and then dried in an oven at 75 °C for 24 h to obtain the AlOOH precursor. The obtained AlOOH was further calcined in an air atmosphere at 420 °C for 8 h to obtain Al_2O_3 nanosheets.

3.3. Preparation of PTCDA/ Al_2O_3 (Physical Mixture)

Typically, the synthesis process of 5%PTCDA/ Al_2O_3 is as follows: 0.0105 g of PTCDA is mixed with 0.2 g of Al_2O_3 , thoroughly grinding in a mortar until the material is evenly mixed, resulting in a composite material of PTCDA and Al_2O_3 , labeled as 5%PTCDA/ Al_2O_3 (physical mixture). A series of x%PTCDA/ Al_2O_3 was also fabricated by changing the mass percentages of PTCDA, where x denotes 1, 3, 5, and 10, respectively.

3.4. General Procedure for the Photocatalytic Selective Oxidation of Sulfide

As is typical, 10 mg of photocatalyst, 1 mL of methanol, and 0.1 mmol of substrate were added to a 10 mL of Pyrex reactor. Then, the reactor was purged with O_2 for 1 min and maintained at 1 atmosphere. And the reactor was placed in an oil bath at 30 °C for 6 h. Afterwards, 0.01 mmol of 1,3,5-trimethoxybenzene was added as the internal standard, and then the photocatalyst was filtered. The conversion and yield of benzyl sulfoxide were determined using Agilent Technologies 7820 gas chromatography equipped with a WondaCap 5 column with anisole as the internal standard. The conversion and yield of other products were determined by ^1H NMR spectra, with 1,3,5-trimethylbenzene as internal standard.

3.5. Characterizations

The XRD patterns were obtained using a Rigaku Ultima IV X-RAY diffractometer with $\text{Cu K}\alpha$ radiation ($\lambda = 1.5418 \text{ \AA}$) in the 2θ range from 5 to 80° at a scanning rate of 8° min^{-1} . Transmission electron microscopy (TEM) measurements were carried out using a JEOL F200 microscope (JEOL, Tokyo, Japan) with an accelerating voltage of 200 kV. X-ray photoelectron spectroscopy (XPS) was conducted using an Escalab 250Xi spectrometer at (Thermo, Waltham, MA, USA) room temperature with an $\text{Al K}\alpha$ X-ray source ($h\nu = 1486.6 \text{ eV}$). The C 1s peak at 284.8 eV was used as the reference for the calibration of the binding energy. UV-vis diffuse reflectance spectra were measured on an Agilent Technologies Cary Series UV-vis-NIR spectrometer (Agilent, Santa Clara, CA, USA). Fourier Transform infrared spectroscopy (FTIR) measurements were made using a Bruker VERTEX 70v spectrometer (Bruker, Billerica, MA, USA). Diffuse reflectance infrared Fourier transform spectroscopy (DRIFTS) measurements were made using a Bruker Tensor II spectrometers (Bruker, Billerica, MA, USA).

3.6. Computational Details

All calculations were performed in the framework of the density functional theory (DFT), with the projector-augmented plane-wave method, as implemented in the Vienna ab initio simulation package (VASP) [21]. The (111) surface was chosen as the active surface to represent the as-prepared $\gamma\text{-Al}_2\text{O}_3$ in our calculation model. The vdW interactions were included using the DFT-D2 method of Grimme [22]. The cut-off energy was set to 400 eV. The energy criterion was set to 10^{-5} eV in the iterative solution of the Kohn–Sham equation.

The Brillouin zone integration was performed using a $2 \times 2 \times 1$ k-mesh. All the structures were relaxed until the residual forces on the atoms had declined to less than $0.02 \text{ eV}/\text{\AA}$.

4. Conclusions

In summary, a quite simple immobilization strategy was applied to modify the PTCDA molecules, which furnished heterogenized PTCDA with remarkably enhanced reactivity and excellent recyclability. Our studies revealed that the simple grinding procedure could induce a strong interaction between the anhydride group of PTCDA and the hydroxyl group of Al_2O_3 . Al_2O_3 with Lewis acidity provided anchoring sites for reagents to significantly facilitate the electron transfer from reagent to PTCDA*, thus greatly improving the overall performance. This work provides new insights for the low-cost production of superior heterogenized molecular photocatalysts, which lays a foundation for large-scale photosynthesis of fine chemicals and pharmaceuticals using molecular photocatalysts.

Supplementary Materials: The following supporting information can be downloaded at: <https://www.mdpi.com/article/10.3390/molecules29091934/s1>, Figure S1. Comparison of activity of series photocatalysts; Figure S2. UV-vis absorption spectra of PTCDA and Al_2O_3 ; Figure S3. (a) DRIFTS spectra of Al_2O_3 , PTCDA/ Al_2O_3 (physical mixture), and PTCDA/ Al_2O_3 (physical mixture)–300, (b) DRIFTS spectra of PTCDA and PTCDA calcined at $300 \text{ }^\circ\text{C}$ (PTCDA–300), (c) DRIFTS spectra of PTCDA and PTCDA calcined at $300 \text{ }^\circ\text{C}$ (PTCDA–300); Figure S4. FTIR spectra of Al_2O_3 , PTCDA, and 5%PTCDA/ Al_2O_3 (physical mixture) adsorbing methanol; Figure S5. (a) Evaluation of photocatalytic stability, (b) FTIR spectra of 5%PTCDA/ Al_2O_3 (physical mixture) before and after reaction; Table S1. Control experiments to study photocatalytic sulfide oxidation; Table S2. Control experiments to study photocatalytic sulfide oxidation.

Author Contributions: Conceptualization, J.L., J.W., H.S. and C.S.; methodology, J.L.; validation, J.W., H.S. and C.S.; formal analysis, J.L., H.H., W.L. and Q.X.; investigation, J.L., H.H., W.L. and Q.X.; data curation, J.L., H.H., W.L. and Q.X.; writing—original draft preparation, J.L. and J.W.; writing—review and editing, J.W., H.S. and C.S.; supervision, J.W., H.S. and C.S.; project administration, H.S. and C.S.; funding acquisition, H.S. and C.S. All authors have read and agreed to the published version of the manuscript.

Funding: This work was supported by the Strategic Priority Research Program of the Chinese Academy of Sciences (XDB36030200), NSFC Center for Single-Atom Catalysis (22388102) and Photon Science Research Center for Carbon Neutrality, the National Key Research and Development Program of China (2021YFA1600800), National Natural Science Foundation of China (21972094, 22102102, 22372102), Educational Commission of Guangdong Province (839-0000013131), Shenzhen Science and Technology Program (RCJC20200714114434086), the City University of Hong Kong start up fund, and the Guangdong Basic and Applied Basic Research Foundation (2020A1515010982), China Postdoctoral Science Foundation (2023M742395), Shenzhen Science and Technology Program (20231122120657001), and Shenzhen University Start Up Fund, Shenzhen Peacock Plan (Nos. 20210308299C).

Institutional Review Board Statement: Not applicable.

Informed Consent Statement: Not applicable.

Data Availability Statement: Data are contained within the article or Supplementary Materials.

Conflicts of Interest: The authors declare no conflicts of interest.

References

1. Ghosh, I.; Ghosh, T.; Bardagi, J.I.; Konig, B. Reduction of aryl halides by consecutive visible light-induced electron transfer processes. *Science* **2014**, *346*, 725–728. [[CrossRef](#)] [[PubMed](#)]
2. Corrigan, N.; Shanmugam, S.; Xu, J.; Boyer, C. Photocatalysis in organic and polymer synthesis. *Chem. Soc. Rev.* **2016**, *45*, 6165–6212. [[CrossRef](#)] [[PubMed](#)]
3. Guo, Y.; Zhou, Q.; Nan, J.; Shi, W.; Cui, F.; Zhu, Y. Perylenetetracarboxylic acid nanosheets with internal electric fields and anisotropic charge migration for photocatalytic hydrogen evolution. *Nat. Commun.* **2022**, *13*, 2067. [[CrossRef](#)] [[PubMed](#)]
4. Wang, X.; Meng, J.; Yang, X.; Hu, A.; Yang, Y.; Guo, Y. Fabrication of a perylene tetracarboxylic diimide-graphitic carbon nitride heterojunction photocatalyst for efficient degradation of aqueous organic pollutants. *ACS Appl. Mater. Interfaces* **2019**, *11*, 588–602. [[CrossRef](#)] [[PubMed](#)]

5. Li, C.; Wonneberger, H. Perylene imides for organic photovoltaics: Yesterday, today, and tomorrow. *Adv. Mater.* **2012**, *24*, 613–636. [[CrossRef](#)] [[PubMed](#)]
6. Zhang, Z.; Chen, X.; Zhang, H.; Liu, W.; Zhu, W.; Zhu, Y. A highly crystalline perylene imide polymer with the robust built-in electric field for efficient photocatalytic water oxidation. *Adv. Mater.* **2020**, *32*, e1907746. [[CrossRef](#)] [[PubMed](#)]
7. Chen, P.; Blaney, L.; Cagnetta, G.; Huang, J.; Wang, B.; Wang, Y.; Deng, S.; Yu, G. Degradation of ofloxacin by perylene diimide supramolecular nanofiber sunlight-driven photocatalysis. *Environ. Sci. Technol.* **2019**, *53*, 1564–1575. [[CrossRef](#)] [[PubMed](#)]
8. Wei, X.; Wang, C.C.; Li, Y.; Wang, P.; Wei, Q. The Z-scheme NH₂-UiO-66/PTCDA composite for enhanced photocatalytic Cr(VI) reduction under low-power LED visible light. *Chemosphere* **2021**, *280*, 130734. [[CrossRef](#)] [[PubMed](#)]
9. Sheng, Y.; Li, W.; Xu, L.; Zhu, Y. High photocatalytic oxygen evolution via strong built-in electric field induced by high crystallinity of perylene imide supramolecule. *Adv. Mater.* **2022**, *34*, 2102354. [[CrossRef](#)]
10. Zhang, Y.; Wang, D.; Liu, W.; Lou, Y.; Zhang, Y.; Dong, Y.; Xu, J.; Pan, C.; Zhu, Y. Create a strong internal electric-field on PDI photocatalysts for boosting phenols degradation via preferentially exposing π -conjugated planes up to 100%. *Appl. Catal. B Environ.* **2022**, *300*, 120762. [[CrossRef](#)]
11. Ronconi, F.; Syrgiannis, Z.; Bonasera, A.; Prato, M.; Argazzi, R.; Caramori, S.; Cristino, V.; Bignozzi, C.A. Modification of nanocrystalline WO₃ with a d Perylene bisimide: Applications to molecular level solar water splitting. *J. Am. Chem. Soc.* **2015**, *137*, 4630–4633. [[CrossRef](#)]
12. Godlewski, S.; Prauzner-Bechcicki, J.S.; Glatzel, T.; Meyer, E.; Szymoński, M. Transformations of PTCDA structures on rutile TiO₂ induced by thermal annealing and intermolecular forces. *Beilstein J. Nanotechnol.* **2015**, *6*, 1498–1507. [[CrossRef](#)]
13. Li, W.; Zhang, H.; Huang, S.; Xu, J.; Liu, L.; Li, J.; Jing, J.; Zhu, Y. Electron-enriched supramolecular PDI-SiO₂ promoting PDS activation for enhanced photocatalytic advanced oxidation. *Appl. Catal. B Environ.* **2024**, *340*, 123262. [[CrossRef](#)]
14. Liu, X.; Ding, X.; An, S.; Wang, X.; Xue, Y.; Zhang, X.; Tian, J. S-scheme enhanced photocatalysis on graphitic carbon nitride functionalized with perylene tetracarboxylic diimide. *Appl. Surf. Sci.* **2023**, *614*, 156273. [[CrossRef](#)]
15. Zhang, J.; Zhao, X.; Wang, Y.; Gong, Y.; Cao, D.; Qiao, M. Peroxymonosulfate-enhanced visible light photocatalytic degradation of bisphenol A by perylene imide-modified g-C₃N₄. *Appl. Catal. B Environ.* **2018**, *237*, 976–985. [[CrossRef](#)]
16. Wei, J.; Chen, X.; Ren, X.; Tian, S.; Bai, F. Facile construction of intramolecular g-CN-PTCDA donor-acceptor system for efficient CO₂ photoreduction. *Catalysts* **2023**, *13*, 600. [[CrossRef](#)]
17. Lv, J.G.; Wang, D.; Peng, L.M.; Guo, X.F.; Ding, W.P.; Yang, W.M. Ethanol dehydration to ethylene over high-energy facets exposed gamma alumina. *Catalysts* **2023**, *13*, 994. [[CrossRef](#)]
18. Li, S.-Q.; Liu, Y.; Li, Y.-L.; Hao, Y.-J.; Liu, R.-H.; Chen, L.-J.; Li, F.-T. Development of γ -Al₂O₃ with oxygen vacancies induced by amorphous structures for photocatalytic reduction of CO₂. *Chem. Commun.* **2022**, *58*, 11649–11652. [[CrossRef](#)]
19. Su, K.; Zhang, C.; Wang, Y.; Zhang, J.; Guo, Q.; Gao, Z.; Wang, F. Unveiling the highly disordered NbO₆ units as electron-transfer sites in Nb₂O₅ photocatalysis with N-hydroxyphthalimide under visible light irradiation. *Chin. J. Catal.* **2022**, *43*, 1894–1905. [[CrossRef](#)]
20. Yang, Z.; Zhang, S.; Zhao, H.; Li, A.; Luo, L.; Guo, L. Subnano-FeO_x clusters anchored in an ultrathin amorphous Al₂O₃ nanosheet for styrene epoxidation. *ACS Catal.* **2021**, *11*, 11542–11550. [[CrossRef](#)]
21. Perdew, J.P.; Burke, K.; Ernzerhof, M. Generalized gradient approximation made simple. *Phys. Rev. Lett.* **1996**, *77*, 3865–3868. [[CrossRef](#)]
22. Chen, D.; Lei, X.; Wang, Y.; Zhong, S.; Liu, G.; Xu, B.; Ouyang, C. Tunable electronic structures in BP/MoSSe van der Waals heterostructures by external electric field and strain. *Appl. Surf. Sci.* **2019**, *497*, 143809. [[CrossRef](#)]

Disclaimer/Publisher's Note: The statements, opinions and data contained in all publications are solely those of the individual author(s) and contributor(s) and not of MDPI and/or the editor(s). MDPI and/or the editor(s) disclaim responsibility for any injury to people or property resulting from any ideas, methods, instructions or products referred to in the content.